End plate stability in thermally-improved steel cladding details

Kara D. Peterman[1], Mark D. Webster[2], James A. D'Aloisio[3], Jerome F. Hajjar[4]

Abstract

Cladding details in steel structures that span the building envelope are particularly prone to thermal transfer, resulting in potential energy loss and condensation. In an attempt to effectively identify and mitigate these thermal bridges, a multi-year research effort was conducted to form design recommendations for practitioners based on thermal modeling, extensive experimental work, and computational modeling. While the project encompassed the thermal mitigation and structural performance of three principal cladding details—slab-supported shelf angles, roof posts, and canopy beams—this paper examines the difference in end plate stability between mitigated and unmitigated roof posts and canopy beams. To this end, cyclic and monotonic testing was conducted on mitigated and unmitigated details under combined axial and lateral load for the roof posts, and lateral load only for the canopy beams. Specimens were instrumented to capture end plate stability modes, post and beam curvature, anchor bolt forces, and strain in the end plates, posts, and beams. While analyses of the data do highlight variation in behavior, results presented herein suggest that the thermally-improved details perform commensurately to the unmitigated details.

1. Introduction to structural thermal breaks

This research is part of a larger effort which explores approaches for developing thermal breaks to mitigate energy loss in steel building structures. This energy loss is formed by structural steel elements that pass through the building envelope, which can potentially act as thermal bridges due to their ability to conduct heat. Thus, heating and cooling are transferred to the exterior and interior, which increases building energy consumption and can contribute to condensation and reduced building occupant comfort. The aim of this project is to explore and validate several structural thermal break concepts and develop associated design recommendations for mitigating the loss of energy and other related issues in steel building structures. By identifying critical details susceptible to becoming thermal bridges, proposing realistic and constructible mitigation strategies, and validating these strategies experimentally and computationally, the work aims to propose solutions for practicing engineers.

---

[1] Assistant Professor, University of Massachusetts Amherst, formerly Postdoctoral Research Associate, Northeastern University <kdpeterman@umass.edu>
[2] Senior Staff II - Structures, Simpson, Gumpertz, and Heger, <mdwebster@sgh.com>
[3] Principal, Klepper Hahn and Hyatt, <jad@khhpc.com>
[4] CDM Smith Professor and Chair, Northeastern University, <jf.hajjar@neu.edu>

The scope of this work includes investigation of structural steel shelf angle details to support building cladding, structural steel roof posts to support dunnage on building roofs, and cantilevered structural steel beams to support light canopies. Experimental testing at the material, connection, and sub-system level was conducted to characterize the performance of these cladding systems, with and without thermal break mitigation. While myriad solutions were proposed, the use of fiber reinforced polymer (FRP) shims at the cladding connection to the building interior have proven particularly effective (Peterman et al 2016) both thermally and structurally. This paper focuses on one component of this validation: the base plate stability failures observed in roof post and canopy testing. Shelf angle cladding details, creep performance of FRP materials, and double-lap splice bolted connections with fills, while included in the project as a whole, are not discussed herein. Results and discussion of these topics may be found in Peterman et al (2016).

2. Roof post and canopy beam testing

Roof posts and canopy beams, despite their differences as structural details, are quite similar thermally. Both details represent discrete cladding details, wherein the structural member only spans the building envelope at the connection points. For roof posts and canopy beams, which are typically comprised of a post/beam portion (steel HSS or pipe), end plates, and bolts or welds to the building structural element, this contact through the building envelope occurs at the base plate (Fig 1). Bolts to the supporting structure can also have a significant impact on the magnitude of energy loss (Peterman et al 2016). Discrete cladding details stand opposed to continuous cladding details, such as the slab-supported shelf angle, which is in contact with the floor slab pour stop for the entire perimeter length of the relieving angle.
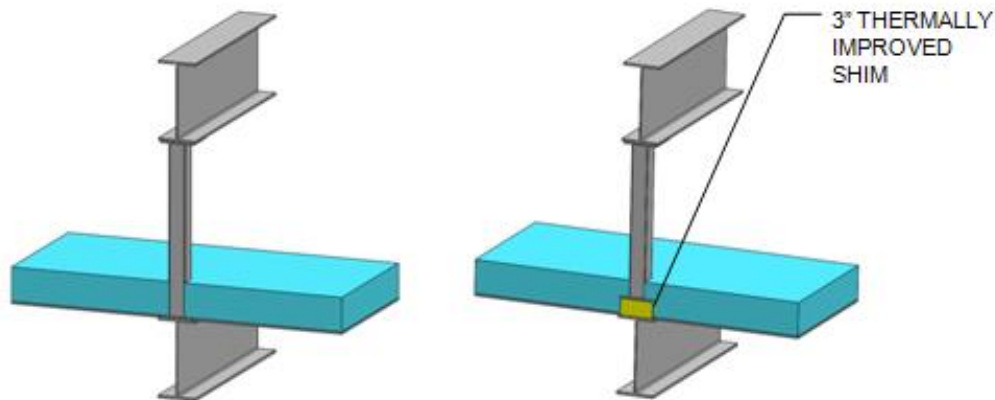

Figure 1: Roof post schematic demonstrating discrete contact with building structural element

As thermally-improved shims (FRP shims in this case) are inserted at the connection, where the thermal bridge is occurring, the effect of these non-steel fills on the sub-system behavior is critical to the development of design recommendations. Roof post and canopy beam systems were tested under cyclic and monotonic loads at the Northeastern University STReSS Laboratory to determine these effects. Five different FRP materials were examined, in varying thicknesses.

2.1 Roof post and canopy beam test matrix

Table 1 presents the test matrix for canopy beams and roof posts. Two design philosophies were employed to assess behavior of these systems, one in which components are overdesigned so that

failure is delayed until well beyond the design envelope, and the other which reflects efficient structural design methods. The overdesigned specimens featured up-sized bolts, welds, and base plates to focus failure towards the shims and post/beam. In the efficiently designed specimens, connections and base plates were designed for factored loads. Shim thickness was varied between 1, 3, and 6 inches, and across vinylester, polyurethane, phenolic, and two proprietary FRP products, determined from discussions with industry representatives to best reflect available materials and common design choices. It should be noted that prior to structural testing, all configurations were modeled in the three-dimensional thermal modeling software package Heat 3 (Blomberg (2001) and Blomberg (2017)) to discern their efficacy as thermal breaks. These results are presented in Peterman et al (2016), but all tested details were determined to be effective at thermal break mitigation strategies.

Table 1: Test matrix for roof post and canopy beam testing (from Peterman et al (2016))

ROOF POSTS (AXIAL + LATERAL)

| Test Name | Specimen Type | MITIGATION STRATEGY | | | SPECIMEN INFORMATION | | | | Loading |
		Type	Material	Thick (in)	End Plate	Rod Dia. (in)	Rod Spacing (in)	Rod Spec	
R1	designed	-	-	-	9x9x3/8"	0.5	6" oc	B8 Class 2	Monotonic
R2	designed	shim	vinylester	3	9x9x1/2"	0.5	6" oc	B8 Class 2	Monotonic
R3	designed	sleeve	FRP 4x4x1/2	-	9x9x3/8"	0.5	6" oc	B8 Class 2	Monotonic
R4	designed	-	-	-	9x9x3/8"	0.5	6" oc	B8 Class 2	Cyclic
R5	designed	shim	vinylester	3	9x9x1/2"	0.5	6" oc	B8 Class 2	Cyclic
R6	designed	sleeve	FRP 4x4x1/2	-	9x9x3/8"	0.5	6" oc	B8 Class 2	Cyclic
R7	over-designed	-	-	-	9x9x1/2"	0.75	6" oc	A307	Cyclic
R8	over-designed	shim	vinylester	3	9x9x1/2"	0.75	6" oc	A307	Cyclic
R9	over-designed	shim	phenolic	3	9x9x1/2"	0.75	6" oc	A307	Cyclic
R10	over-designed	shim	polyurethane	3	9x9x1/2"	0.75	6" oc	A307	Cyclic
R11	over-designed	shim	proprietary 1	3	9x9x1/2"	0.75	6" oc	A307	Cyclic
R12	over-designed	shim	proprietary 2	3	9x9x1/2"	0.75	6" oc	A307	Cyclic
R13	over-designed	shim	vinylester	1	9x9x1/2"	0.75	6" oc	A307	Cyclic
R14	over-designed	shim	vinylester	6	9x9x1/2"	0.75	6" oc	A307	Cyclic

CANOPY BEAMS (LATERAL)

| Test Name | Specimen Type | MITIGATION STRATEGY | | | SPECIMEN INFORMATION | | | | Loading |
		Type	Material	Thick (in)	End Plate	Rod Dia. (in)	Rod Spacing (in)	Rod Spec	
C1	designed	-	-	-	9x9x3/8"	0.75	6" oc	B8 Class 2	Monotonic
C2	designed	shim	vinylester	3	9x9x3/8"	0.75	6" oc	B8 Class 2	Monotonic
C4	designed	-	-	-	9x9x3/8"	0.75	6" oc	B8 Class 2	Cyclic
C5	designed	shim	vinylester	3	9x9x3/8"	0.75	6" oc	B8 Class 2	Cyclic
C7	over-designed	-	-	-	9x9x1/2"	1	6" oc	A307	Cyclic
C8	over-designed	shim	vinylester	3	9x9x1/2"	1	6" oc	A307	Cyclic
C9	over-designed	shim	phenolic	3	9x9x1/2"	1	6" oc	A307	Cyclic
C10	over-designed	shim	polyurethane	3	9x9x1/2"	1	6" oc	A307	Cyclic
C11	over-designed	shim	proprietary 1	3	9x9x1/2"	1	6" oc	A307	Cyclic
C12	over-designed	shim	proprietary 2	3	9x9x1/2"	1	6" oc	A307	Cyclic
C13	over-designed	shim	vinylester	1	9x9x1/2"	1	6" oc	A307	Cyclic
C15	over-designed	shim	vinylester	6	9x9x1/2"	1	6" oc	A307	Cyclic

In accordance with industry standards, and representing common configurations for their respective details, roof posts were designed to be 30 inches in height while canopy beams were designed to be 66 inches in height. To maintain symmetry in experimental testing, base plates (which may be rectangular or square) were designed as square and using the recommendations outlined in the AISC Base Plate Design Guide (AISC 2006). However, to explore a range of potential responses in the base conditions, efficiently-designed specimens were thinner than the industry standard, which is typically ¾" (AISC 2006) and significantly overdesigned for the factored loads. Bolts were placed on the base plate at 6" on center, and were both efficiently

designed with thermally-superior stainless steel B8 Class 2 bolts, and overdesigned with 1" dia. A307 bolts (again, in accordance with industry practices). Bolts were installed by a single operator and were specified as snug-tight. Holes were specified as standard holes. Specimen drawings are shown in Fig 2 below for the designed configurations, along with a photograph of a canopy beam specimen in the test rig.

Roof posts were designed as HSS 3x3x3/16 while canopy beams were designed as HSS 4x4x1/2 (all HSS were specified as ASTM A500, Grade B (46 ksi)). Welds between the post or beam and its base plate typically had the potential to be the critical limit state in these details, and as such, were detailed as complete joint penetration (CJP) welds to ensure they did not impact response in the design regime. Thus, CJP welds were used regardless whether the specimen was overdesigned or efficiently-designed.
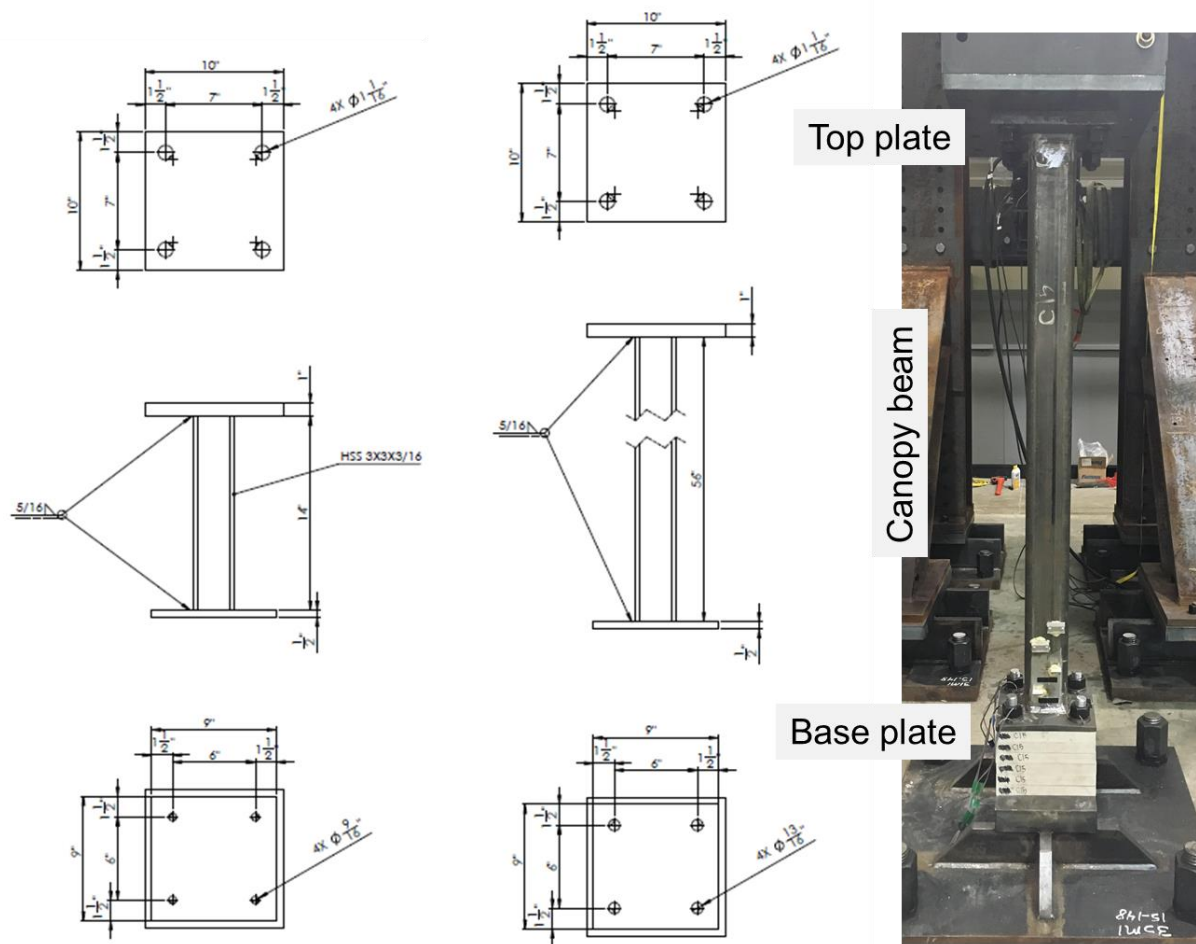

Figure 2: Roof post (left) and canopy beam (center) specimen schematics, specimen as installed in rig at right.

2.2 Test setup and loading protocol

The roof post/canopy beam test rig is comprised of two actuators, one lateral and one vertical, a load transfer block, the base (connecting specimen to the strong floor), and the reaction frame. These components are illustrated in Figure 3 below.

Roof posts are initially loaded with a 10 kip axial load to replicate the weight of typical dunnage on the post. After the axial load is applied via the vertical actuator in load control, the horizontal actuator loads the specimen in displacement control. Regardless of lateral displacements, the axial load remains constant throughout the duration of the test. Canopy beams are intended to be pure cantilevers with zero axial force. To achieve this condition, the vertical actuator counteracts the weight of the load transfer block and half of the horizontal actuator so that the total axial force on the specimen is zero. In both the roof post and canopy beam test setups, the load transfer block is allowed to rotate to simulate a cantilever boundary condition, and is only restrained in the out-of-plane dimension (refer to Peterman et al (2016) for test rig schematics and detail drawings).

Load is applied to the top of the specimen (connected to a 1" end plate via a CJP weld) via a load transfer block, which connects the two actuators to the top of the specimen and is assumed to be rigid. The horizontal and vertical actuators are connected to steel frames which are vertically adjustable.
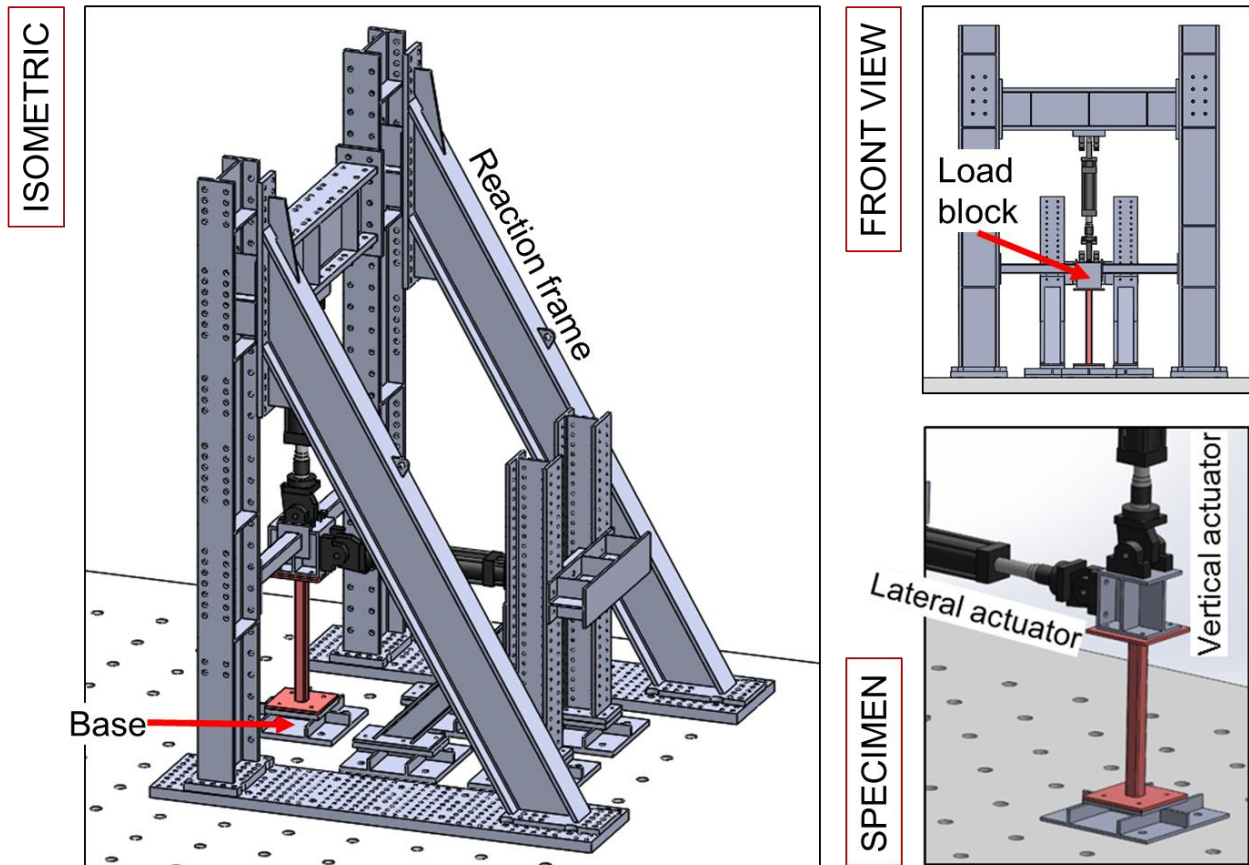

Figure 3: Test rig schematics, illustrating rig components and specimen installation

Monotonic tests were displacement-controlled for the horizontal actuator, at a rate of 0.18% drift per minute. The vertical actuator was force-controlled throughout testing. Cyclic tests were displacement-controlled for the horizontal actuator, loading at a rate of 2.1% drift per minute, while the vertical actuator remained in load-control (Gomez et al (2009) conducted similar

experiments on steel posts with base plates; load rates are taken from that experimental program). The SAC protocol (Krawinkler, 1996) was used for the cyclic testing, and was scaled to the exact height of each specimen (which varied due to differing shim thicknesses) which ensured constant load rate and drift targets across all testing.

2.3 Instrumentation plan

To capture lateral movement of the base plate, linear variable differential transducers (LVDTs) were installed on the West face of the base plate (shown in Figure 4 below, with cardinal directions and experimental orientation defined) and were affixed to stiff magnetic fixtures installed on the rig base. Quintuplet LVDTs on the south and east sides of the base plate were oriented vertically to record the buckling of the base plate along its face on these two sides of the member, one in the loaded direction and the other in the transverse direction. Specimens were assumed to behave symmetrically. These quintuplet sensors recorded base plate deformed shapes up until approximately 2% drift, where large deformations in the base plate typically resulted in misalignment of the sensors and occasionally loss of contact with the base plate. At this point, the quintuplet sensors were removed from the specimen.
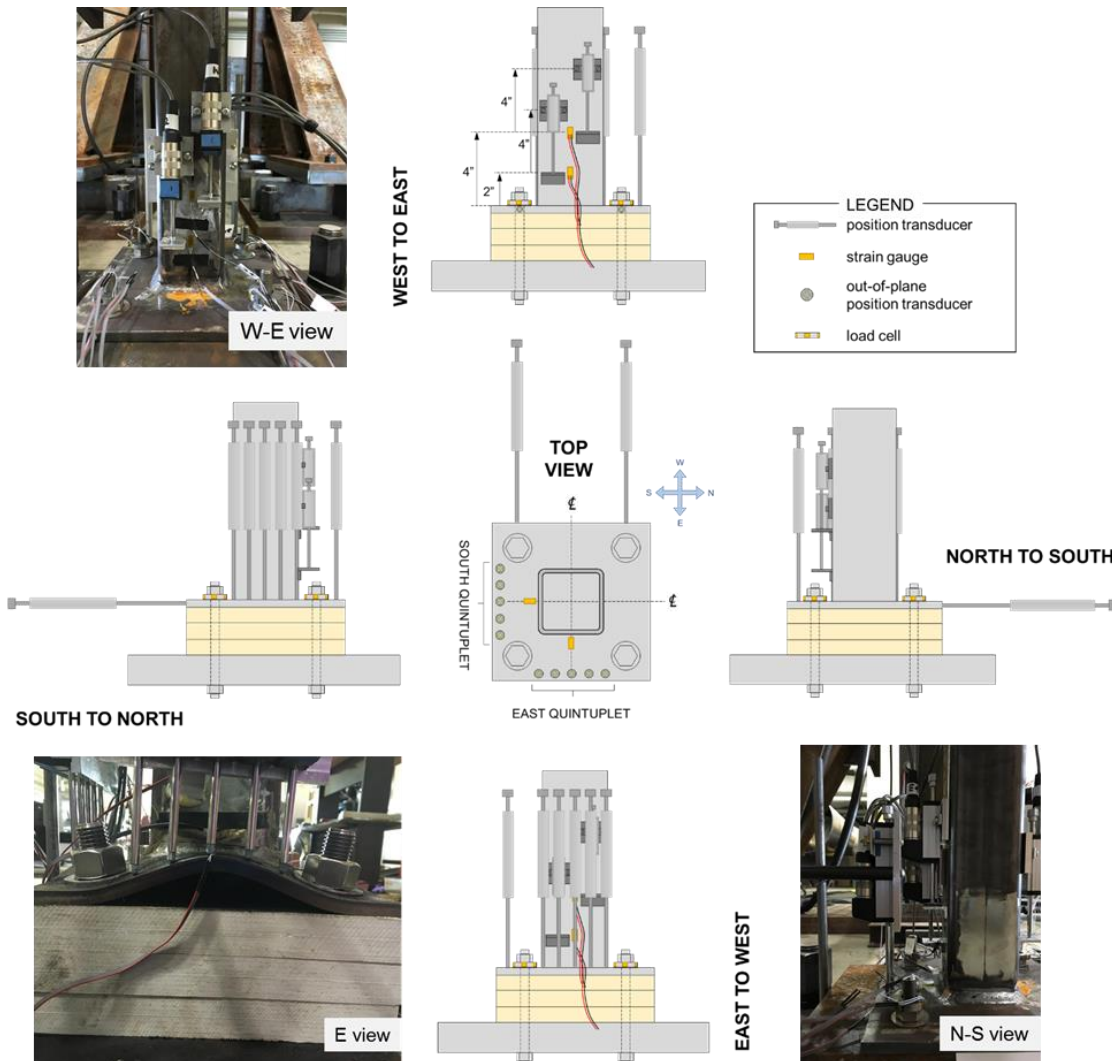

Figure 4: Instrumentation plan and photographs of sensors installed on a deformed specimen.

6

Using small LVDTs installed along the vertical dimension of the post/beam, it is possible to calculate curvature of the post. Two LVDTs were installed along the east and west faces of the HSS specimens, overlapping such that their gage lengths were staggered, and were mounted to the HSS via aluminum brackets adhered to the specimen. Strain gauges were also installed on each specimen, with one on the south and east faces of the base plate, 1" away from the weld to the post. Strain gauges at 2" and 4" up from the base plate were installed on the post/beam on the west and east sides of the specimen.

3. Results and discussion

Roof post and canopy beam results are presented are presented in Table 2 and 3 respectively. Maximum experimental loads and moments are included, as well as base plate, post bending, shim compression, bolt tension, bolt shear, and bolt bending limit states. Results are presented for the system, i.e., four bolts are considered for shear and bending calculations. In the case of bolt tension, two bolts are considered under uplift only (caused by bending of the post). Rf, a reduction factor to account for experimental end conditions (used as a multiplier on post/beam inflection point for moment calculations), is provided and is detailed in Peterman et al (2016).

Table 2: Roof post results and nominal strength-to-predicted ratios (from Peterman et al 2016)

ROOF POSTS - NOMINAL

	STRENGTH RESULTS				BASE PLATE YIELDING			POST BENDING	
Test	P_{max}	R_f	h	M_u	P_n	P_u	P_u/P_n	M_n	M_u/M_n
Name	kip	-	in	kip-in	kip	kip	-	kip-in	-
R1	5.33	0.85	21	95.21	15.40	5.33	0.35	90.84	1.05
R2	8.34	0.85	21	148.85	27.38	8.34	0.30	90.84	1.64
R3	4.39	1	21	92.19	15.40	4.39	0.29	90.84	1.01
R4	5.57	0.85	21	99.37	15.40	5.57	0.36	90.84	1.09
R5	8.69	0.85	15	110.80	27.38	8.69	0.32	90.84	1.22
R6	5.88	1	15	88.20	15.40	5.88	0.38	90.84	0.97
R7	6.88	0.95	21	137.26	27.38	6.88	0.25	90.84	1.51
R8	9.29	0.95	15	132.38	27.38	9.30	0.34	90.84	1.46
R9	6.44	0.95	15	91.74	27.38	6.44	0.24	90.84	1.01
R10	9.44	0.95	15	134.52	27.38	9.44	0.34	90.84	1.48
R11	9.29	0.95	15	132.31	27.38	9.29	0.34	90.84	1.46
R12	9.04	0.95	15	128.83	27.38	9.04	0.33	90.84	1.42
R13	9.31	0.95	15	132.67	27.38	9.31	0.34	90.84	1.46
R14	8.69	0.95	15	123.83	27.38	8.69	0.32	90.84	1.36

	BOLT TENSION			BOLT SHEAR			BOLT BENDING		
Test	T_{bn}	T_{uplift}	T_{uplift}/T_{bn}	T_n	F_{act}	F_{act}/T_n	M_{bu}	M_{bn}	M_{bu}/M_{bn}
Name	kip	kip	-	kip	kip	-	kip-in	kip-in	-
R1	30.63	15.87	0.52	36.91	5.33	0.14	-	1.91	-
R2	30.63	24.81	0.81	36.91	8.34	0.23	25.02	1.91	13.068
R3	30.63	15.37	0.50	36.91	4.39	0.12	-	1.91	-
R4	30.63	16.56	0.54	36.91	5.57	0.15	-	1.91	-
R5	30.63	18.47	0.60	36.91	8.69	0.24	26.07	1.91	13.618
R6	30.63	14.70	0.48	36.91	5.88	0.16	-	1.91	-
R7	39.76	22.88	0.58	47.71	6.88	0.14	-	3.73	-
R8	39.76	22.08	0.56	47.71	9.30	0.19	27.89	3.73	7.4815
R9	39.76	15.29	0.38	47.71	6.44	0.13	19.31	3.73	5.1814
R10	39.76	22.42	0.56	47.71	9.44	0.20	28.32	3.73	7.5974
R11	39.76	22.05	0.55	47.71	9.29	0.19	27.86	3.73	7.4727
R12	39.76	21.47	0.54	47.71	9.04	0.19	27.12	3.73	7.2763
R13	39.76	22.11	0.56	47.71	9.31	0.20	9.31	3.73	2.4976
R14	39.76	20.64	0.52	47.71	8.69	0.18	52.14	3.73	13.988

Table 3: Canopy beam results and nominal strength-to-predicted ratios (from Peterman et al 2016)

CANOPY BEAMS - NOMINAL

	STRENGTH RESULTS				BASE PLATE YIELDING			POST BENDING	
Test	P_{max}	R_f	h	M_u	P_n	P_u	P_u/P_n	M_n	M_u/M_n
Name	kip	-	in	kip-in	kip	kip	-	kip-in	-
C1	4.887	0.8	57	222.85	13.92	4.89	0.35	354.60	0.63
C2	5.807	0.8	51	236.93	13.92	5.81	0.42	354.60	0.67
C4	4.539	0.8	57	206.98	13.92	4.54	0.33	354.60	0.58
C5	4.858	0.8	51	198.21	13.92	4.86	0.35	354.60	0.56
C7	6.213	0.95	57	336.43	24.75	6.21	0.25	354.60	0.95
C8	7.04	0.95	51	341.09	24.75	7.04	0.28	354.60	0.96
C9	6.752	0.95	51	327.13	24.75	6.75	0.27	354.60	0.92
C10	7.236	0.95	51	350.58	24.75	7.24	0.29	354.60	0.99
C11	6.962	0.95	51	337.31	24.75	6.96	0.28	354.60	0.95
C12	7.176	0.95	51	347.68	24.75	7.18	0.29	354.60	0.98
C13	7.032	0.95	51	340.70	24.75	7.03	0.28	354.60	0.96
C15	6.804	0.95	51	329.65	24.75	6.80	0.27	354.60	0.93

	BOLT TENSION			BOLT SHEAR			BOLT BENDING		
Test	T_{bn}	T_{uplift}	T_{uplift}/T_{bn}	T_n	F_{act}	F_{act}/T_n	M_{bu}	M_{bn}	M_{bu}/M_{bn}
Name	kip	kip	-	kip	kip	-	kip-in	kip-in	-
C1	68.92	37.14	0.54	83.06	4.89	0.06	-	6.46	-
C2	68.92	39.49	0.57	83.06	5.81	0.07	17.42	6.46	2.70
C4	68.92	34.50	0.50	83.06	4.54	0.05	-	6.46	-
C5	68.92	33.03	0.48	83.06	4.86	0.06	14.57	6.46	2.26
C7	70.69	56.07	0.79	84.82	6.21	0.07	-	8.84	-
C8	70.69	56.85	0.80	84.82	7.04	0.08	21.12	8.84	2.39
C9	70.69	54.52	0.77	84.82	6.75	0.08	20.26	8.84	2.29
C10	70.69	58.43	0.83	84.82	7.24	0.09	21.71	8.84	2.46
C11	70.69	56.22	0.80	84.82	6.96	0.08	20.89	8.84	2.36
C12	70.69	57.95	0.82	84.82	7.18	0.08	21.53	8.84	2.44
C13	70.69	56.78	0.80	84.82	7.03	0.08	7.03	8.84	0.80
C15	70.69	54.94	0.78	84.82	6.80	0.08	40.82	8.84	4.62

Base plate yielding is characterized by yield line diagrams, and relationships for the yield load on the plate are determined from the diagram geometry, as shown in Figure 5 below. Given that all of the base plates tested in the study deformed significantly and buckled on the loaded side (east only for monotonic tests, east and west for cyclic tests), this method is thought to be overly conservative, and test-to-predicted ratios are well below 1. The equations developed for these yield forces are shown in Figure 5 below.

$$P = \frac{73 F_y t^2}{24} \quad \text{HSS 3x3x3/16}$$

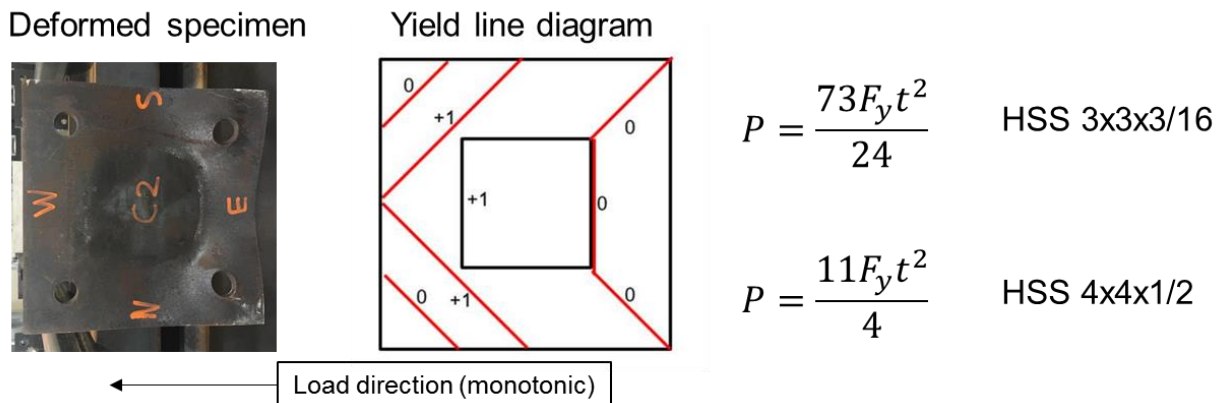$$P = \frac{11 F_y t^2}{4} \quad \text{HSS 4x4x1/2}$$

Figure 5: Yield line diagram for base plates and post/beams, based on observed deformed shapes (deformed specimen C2 shown at left, photograph is of bottom of base plate)

Shim compression for roof posts is determined via a combination of the applied axial force (10 kips) and the compression due to bending moment at the base plate at the maximum force. For canopy beams, which do not have applied axial load, shim compression is based solely on the compressive stresses from bending of the beam.

Based on the tabulated test-to-predicted ratios, bolt bending governs, and is magnified with shims of increasing thickness. However, it should be noted that design moments for roof posts are approximately 5 kip-ft (60 kip-inches) during which the specimen responses are still elastic, so all specimens resisted loads well in excess of the design loads.

Figure 6 highlights typical failure modes observed from roof post and canopy beam testing. Base plate bending on both loaded and transverse edges occurred first in the test, regardless of base plate thickness. Despite initial buckling of the base plate, the specimens were able to maintain increasing strength until fracture of the post/beam in the heat affected zone (HAZ) of the CJP weld resulted in rapid strength drops. These fractures occurred well beyond the design regime for the roof posts and canopy beams. Shims were structurally undamaged, and only experienced friction from the base plate which resulted in paint flaking and cosmetic damage.
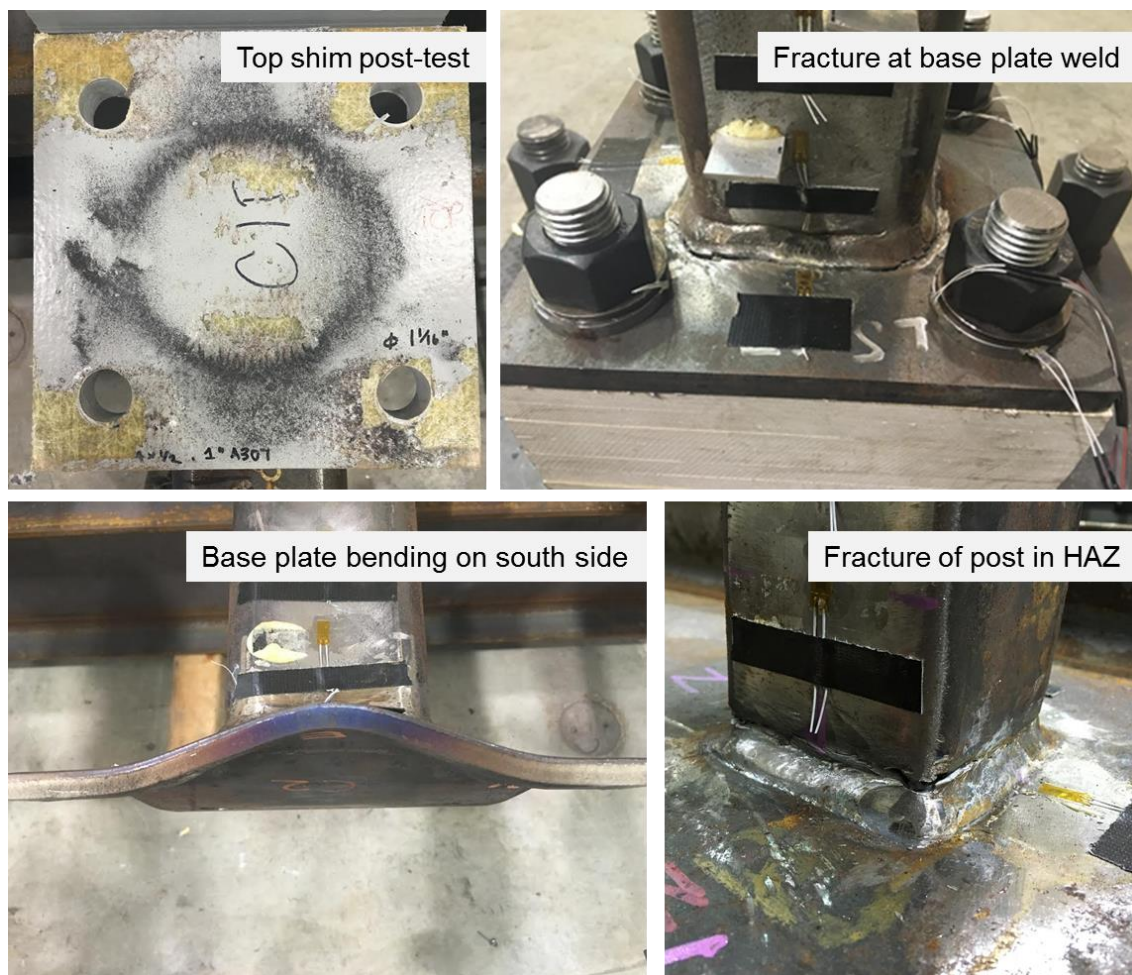
Figure 6: Photographs of typical failure modes for roof posts and canopy beams (from Peterman et al 2016)

4. Conclusions

Canopy beams and roof posts with shims between the base plate and the support structure may be designed using typical industry practices modified to account for the shims. While thin base plates and subsequent stability failures did impact the progression of damage and ultimate capacity of the subsytems, under design loads, the efficiently designed specimens performed adequately, with and without FRP shims. The presence of FRP fills in the bolted connections did not impact stiffness of the system, and only produced slight variations in maximum force and moment. These variations were consistent with differences in strength between FRP materials. These strengths are documented and discussed thoroughly in Peterman et al (2016). While yield lines were used to provide predictions for base plate bending modes, it is necessary to better encapsulate this failure mode via improved analytical expressions.

References

American Institute of Steel Construction (AISC) (2005). Specification for Structural Steel Buildings, ANSI/AISC 360–05, AISC, Chicago, Illinois.

American Institute of Steel Construction (AISC) (2010). Specification for Structural Steel Buildings, ANSI/AISC 360–10, AISC, Chicago, Illinois.

American Institute of Steel Construction (AISC) (2006). Base Plate and Anchor Rod Design, 2nd ed. AISC, Chicago, Illinois.

Blomberg, T. (2001). "HEAT3 Version 4.0 - A PC-program for Heat Conduction in Three Dimensions," Department of Building Physics, Lund University, Lund, Sweden.

Blomberg, T. (2017). "HEAT3 Version 7.0 - A PC-program for Heat Conduction in Three Dimensions," Department of Building Physics, Lund University, Lund, Sweden.

Gomez, I., Kanvinde, A., Smith, C., Deierlein, G. (2009). Shear Transfer in Exposed Column Base Plates. Report presented to the American Institute of Steel Construction (AISC). March 2009.

Krawinkler, H., (1996). Cyclic loading histories for Seismic Experimentation on Structural Components. Earthquake Spectra, the Professional Journal of the Earthquake Engineering Research Institute, Vol. 12, Number 1, pp 1-12.

Peterman, K.D., Kordas, J.A., Moradei, J., Coleman, K., D'Aloisio J.A., Webster, M.D., Hajjar, J.F. (2016). Thermal Break Strategies for Cladding Systems in Building Structures: Report to the Charles Pankow Foundation. December 30, 2016.